Numerical Study of Non-Linear Effects for a Swept Bias Langmuir Probe

Kai Morgan Kjølerbakken, *Member, IEEE*, Wojciech J. Miloch, *Member, IEEE*, Ørjan Grøttem Martinsen, *Senior Member, IEEE*, Oliver Pabst, *Member, IEEE*, and Ketil Røed, *Member, IEEE*

***Abstract*— We present a numerical study disclosing non-linear effects and hysteresis loops for a swept bias Langmuir probe. A full kinetic particle in cell (PIC) model has been used to study the temporal sheath effects and the probe current. Langmuir probes are normally operated at low frequencies, since a "close to steady state" condition is required to characterize the plasma. However, during operations above frequencies normally used, capacitive and non-linear resistive effects are being unveiled. We demonstrate how ion and electron density and temperature change properties of the probe-plasma system. We also show that a swept Langmuir probe exhibits essential properties described as the "fingerprint of memristors" and how a Langmuir probe can be identified as a transversal memristor. Understanding non-linear processes might enable new ways to operate Langmuir probes with higher sampling rates and better accuracy.**

***Index Terms*— Langmuir probes, memristors, plasma.**

I. Introduction

LANGMUIR probes are standard instruments for characterizing plasma quantities both in space physics and in laboratory experiments. Langmuir probes are inexpensive and relatively easy to operate, and theoretical models to derive electron density and temperature based on the measured voltage–current (V–I) relation have been established. The simplest setup for characterization of plasma is a single Langmuir probe where the probe bias is swept through a voltage range. Since the plasma needs some time to adjust to the voltage and to stabilize, due to sheath formation and sheath capacitance, there will be limitations on the sweeping frequency and subsequently a temporal limitation of the system. Other methods utilizing several Langmuir probes, each with their own fixed bias, have been developed allowing a higher sampling rate [1]. The trade-off is a more complicated setup involving more circuitry that needs to be calibrated. In the ionosphere radio frequency (RF) probes like sweeping impedance probes (SIP) and High Frequency Capacitance probes (HFC) are also used [2]–[4]. While Langmuir probes require a low frequency of the sweep, at which the sheath gets time to establish itself, SIP rely on sweeping frequencies so high that the sheath does not get time to form and the effect of the sheath is negligible [5]. These probes are normally operated in the range from a few hundred kHz to a few dozen MHz, and the data can be analyzed using a fluid formulation and thin sheath approximation [2], [6], [7].

When data from Langmuir probes are analyzed, we often see deviations from theoretical studies [8]. This can be caused by charged objects close to the probes, contamination on the probe itself [9], [10] or the method used for analyzing, including how the data is fit to the measured V–I curve [8]. Relevant for this study is hysteresis effects observed in V–I characteristics, which are commonly contributed to surface contamination and is discussed in numerous studies [11]–[14].

In this article, we study the response of a single spherical Langmuir probe when the sweeping frequency of the probe bias is increased beyond the maximum frequency normally used (which would be required for reaching a steady-state condition), and into the domain where capacitive and non-linear resistive effects are being unveiled. We are still operating at frequencies below the RF probes. Understanding these processes might enable new ways to operate Langmuir probes at higher sampling rates and with better accuracy. Langmuir probes have been used on many sounding rockets, satellites, and interplanetary spacecraft to perform *in situ* measurements of electron/ion density and temperature. In our study, we use realistic parameters typically reflecting a Low Earth Orbit environment of a satellite.

II. Sheath Effects on Langmuir Probes

When operating a probe to obtain the I–V characteristics, the probe needs to be biased relative to floating potential, which is a potential of an isolated object in plasma at which the net current to the object surface vanishes. Thus, the probe potential is swept through a voltage range V, and the corresponding probe current I is measured. We normally require a low sweeping frequency, so the sheaths and the probe current are stable before we do the readout, which is reached within a few ion plasma periods.

Manuscript received September 23, 2021; revised January 25, 2022; accepted March 5, 2022. Date of publication April 14, 2022; date of current version May 11, 2022. This work was supported in part by the 4DSpace Strategic Research Initiative at the University of Oslo; in part by the Research Council of Norway under Grant 275653; and in part by the Abel Cluster and the Sigma2 Cluster, owned by the University of Oslo and Uninett/Sigma2, under Project NN9761K. The work of Wojciech J. Miloch was supported by the European Research Council (ERC) through the European Union's Horizon 2020 Research and Innovation Program under ERC Consolidator Grant Agreement 866357, POLAR-4DSpace. The review of this article was arranged by Senior Editor S. Portillo. *(Corresponding author: Kai Morgan Kjølerbakken.)*

Kai Morgan Kjølerbakken is with the Department of Physics, University of Oslo, 0315 Oslo, Norway, and also with the Norwegian Institute for Air Research, 2007 Kjeller, Norway (e-mail: kaimk@fys.uio.no).

Wojciech J. Miloch, Ørjan Grøttem Martinsen, Oliver Pabst, and Ketil Røed are with the Department of Physics, University of Oslo, 0315 Oslo, Norway.

Color versions of one or more figures in this article are available at https://doi.org/10.1109/TPS.2022.3164220.

Digital Object Identifier 10.1109/TPS.2022.3164220

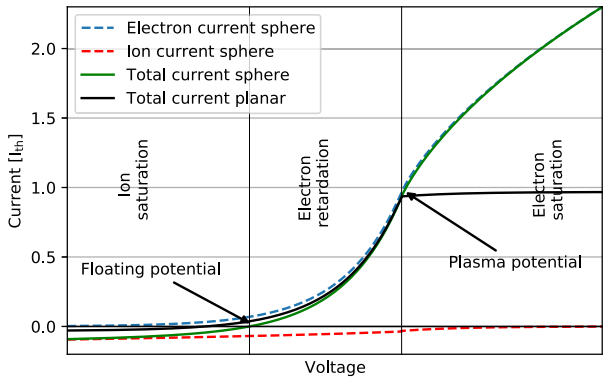

Fig. 1. V–I curve for a Langmuir probe, showing the floating potential, V_f, and the plasma potential V_p. Outside this region, we find the ion saturation region and the electron saturation region. The blue dashed line shows the electron current, the red dashed line shows the ion current and the green solid line shows the total probe current, all for a spherical probe. The black solid line shows the total current for a planar probe.

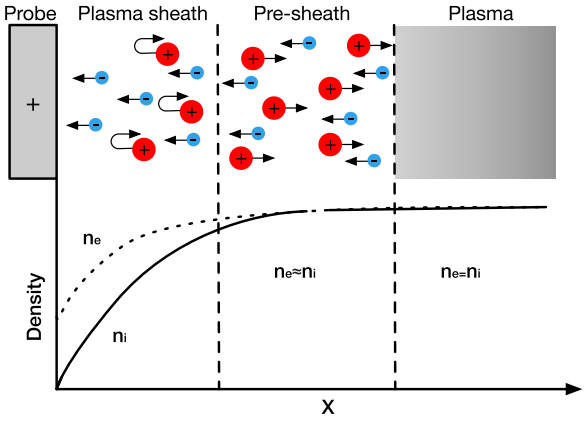

Fig. 2. Plasma probe coupling. For an object with a positive potential the electrons are attracted and the ions are rejected. We can see that the density of the electrons will dominate in the vicinity of the probe and shield out the positive probe potential.

The bias voltage controls whether electrons or ions are repelled or attracted to the probe. For a negative bias voltage, much below the floating potential, the probe will operate in the ion saturation region, where electrons are repelled, and all ions are attracted, see Fig. 1. In this region, a sheath caused by a majority of positively charged ions will build in the vicinity of the probe and limit the ion current. For voltages above floating potential but still beyond the plasma potential the probe will be in the electron retardation region. In this region both the electron and ion densities decrease but at a different rate. Assuming the ions are positively charged, the ion density decreases because ions are attracted by the negative potential while the electrons are repelled. However, to form this negative sheath the ion density must decrease more than the density of the electrons, and for cold ions it must have thermal speed exceeding the Bohm-velocity, v_B, given by [15]

$$v_B = \sqrt{\frac{kT_e}{m_i}} \tag{1}$$

where k is Boltzmann's constant, T_e is the electron temperature, and m_i is the ion mass. In this region, the ion current is negligible and most of the current is determined by the number of electrons which can overcome a retarding potential. The current will have an exponential growth up until it reaches the plasma potential where all sheaths are broken down.

In the electron saturation region, all electrons are attracted and the electron current will be limited, in the same way as the ion current in the ion saturation region, by a non-neutral sheath caused by a majority of negative particles close to the probe as seen in Fig. 2. Outside the sheath region, we have the presheath where quasi-neutrality has been established, but electrons and ions are still accelerated [16]. The sheath will couple the probe potential to the quasi-neutrality plasma where the majority of the particles accelerated toward the probe equals out the potential of the probe. The sheath does not have a sharply defined edge, although, in general, we can assume that outside the sheath region the quasi-neutrality of the plasma is preserved and inside the sheath region the plasma quasi-neutrality brakes down.

The distance where the electric field of an isolated object at floating potential becomes so weak, that the thermal energy of the particles is sufficient to escape from the electrostatic potential is called the Debye length λ_D. It depends on the electron temperature and the electron density, n_e, and it is given by

$$\lambda_D = \sqrt{\frac{k\epsilon_0 T_e}{q_e^2 n_e}} \tag{2}$$

where ϵ_0 is the permittivity of free space.

A. Probe Current

The analytic theory for the probe current was first introduced by orbital-motion-limited (OML) theory by Mott-Smith and Langmuir [17], and it requires a steady-state condition for the sheath and the measured current for each probe bias. The dominating factor is normally the time required for the sheath to form and the time the particles need to traverse the sheath. The OML theory provides a simple formula for calculating electron and ion current for some basic probe shapes: planar, cylindrical, and spherical. It is normally based on a Maxiwellian velocity distribution and assumes a collisionless plasma. From the OML theory the current collected by a Langmuir probe in the saturation regions for a given species s is given by [18]

$$I_s = \mathrm{CI}_{\mathrm{th}}\left(1 + \frac{eV}{kT_s}\right)^{\beta} \tag{3}$$

where the thermal current I_{th} to the probe is given by

$$I_{\mathrm{th}} = n_s q_s \sqrt{\frac{kT_s}{2\pi m_s}} A. \tag{4}$$

Here, A is the surface area of the probe, the parameters C and β are the dependent on the geometry of the probe, where β equals 0, 0.5, and 1 for, respectively, planes, cylinders, and spheres. The parameter C is for a cylindrical probe $C = (2/\sqrt{\pi})$ and for spherical and plane probes $C = 1$. V is the potential of the probe relative to the ambient plasma. For the repelled species, such as for the electrons in the electron retardation region, the collected current will be given by

$$I_e = I_{\mathrm{th}} \exp\left(\frac{eV}{kT_e}\right). \tag{5}$$

III. Temporal Effects for Langmuir Probes

In practice, the applied bias will be a linearly ramped voltage, normally applied by a triangular sawtooth waveform. The frequency must be sufficiently low for the sheaths to be established, and the particles must have time to traverse the sheaths. However, we aim to study how a sinusoidal bias affects the collected current to understand the temporal effects in the transition phase before the probe reaches steady state and look for non-linear properties. A good overview over the temporal effects can be found in the study by Lobbia and Gallimore [19] where five temporally constraining issues are mentioned: 1) sheath transit time; 2) sheath formation time; 3) plasma resonance; 4) polarization drift; and 5) capacitive effects due to sheath capacitance, stray capacitance, and mutual capacitance.

A. Sheath Formation Time

The sheath will couple the probe potential to the quasi-neutral plasma as illustrated in Fig. 2 where the difference in density between negative and positive charges equals out the probe potential toward the quasi-neutral plasma. When the probe potential changes, the sheath changes its size and species composition. While the electrons, due to their higher velocity, adapt rather fast, within a few nanoseconds, the sheath still needs to adjust to the ions. Based on simulation, it has been suggested that the sheath formation time can be between a few and up to ten ion plasma cycles before the sheath has been fully established [20]

$$\tau_{\text{sheath}} \approx 10 f_{\text{ion}}^{-1}. \tag{6}$$

Based on the sheath formation rate, the sheath formation time can also be approximated to [19]

$$\tau_{\text{sheath}} \approx \frac{4V_{\text{sheath}}}{A_{\text{sheath}} v_{\text{ion}}} \tag{7}$$

where, V_{sheath}, is the sheath volume, A_{sheath} is the sheath area and, v_{ion} is ion thermal velocity given by

$$v_{\text{ion}} = \sqrt{\frac{8kT_{\text{ion}}}{m_{\text{ion}}}}. \tag{8}$$

For a spherical probe this can further be expressed by the Debye length, electron temperature, ion mass and the probe radius r_p

$$\tau_{\text{sheath}} \approx 2(r_p + \lambda_D)/\sqrt{eT_e/m_i}. \tag{9}$$

B. Capacitive Effects

Several capacitive sources can be related to a Langmuir probe system, such sources may include: probe-plasma sheath capacitance, stray capacitance between the probe line and the ground level, and mutual capacitance between neighboring conductors.

C. Sheath Capacitance

The shielding caused by the higher mobility of electrons acts like a component with capacitive properties in parallel with the sheath resistance, as seen in Fig. 3. The probe sheath capacitance, C_{sheath}, is in general given by [21]

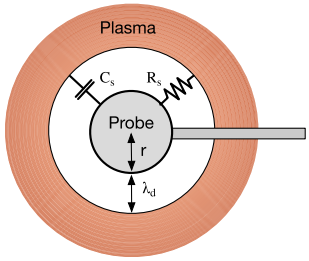

Fig. 3. Spherical Langmuir probe and its coupling to the plasma through the sheath capacitance, C_s, and the sheath resistance, R_s.

$$C_{\text{sheath}} = \alpha \frac{\epsilon_0 A_{\text{probe}}}{\lambda_d} \tag{10}$$

where α is determined by experimental data and will be in the range 0.1–1. For a probe with a spherical geometry where $\lambda_d \gg r$ this can further be expressed as

$$C_{\text{sheath}} = \frac{4\pi\epsilon_0 r_p^2}{\lambda_d}. \tag{11}$$

Typical values for the sheath probe-plasma capacitance for our probe are in the range 5–15 pF. Given the reactance $\chi_c = 1/2\pi f C$, we can see that the current related to the capacitance

$$i = 2\pi f C_{\text{sheath}} V \tag{12}$$

is dependent of both the frequency and the capacitance, and we see that the current will increase with the frequency. Combining (12) with the capacitance given in (10), we see that the current is proportional to $i \propto (1/\lambda_D)$ for $(r/\lambda_d) \gg 1$ and further related to the electron temperature given in (2). We see that the capacitive current, i_c, is inversely proportional to temperature

$$i_c \propto \frac{1}{\sqrt{T_e}} \tag{13}$$

and similarly we see that the current is directly proportional to the density

$$i_c \propto \sqrt{n_e}. \tag{14}$$

The capacitive current will decrease as the electron temperature increases and it will increase as the density increases.

D. Stray Capacitance

In the real setup of a Langmuir probe, stray capacitance will occur. This capacitance arises between the probe line and the ground level of the system and will be in series with the probe. With the intention of reducing complexity, to better understand the non-linear effects, the stray capacitance will be neglected in our model.

IV. Memristive Properties

A memristor links magnetic flux and charge, and its state-dependent resistance which depends on the previous flow of charges. Like a normal resistor, a memristor reduce the flow of charge and has the same unit as normal resistance, Ω [22], [23]. However, a memristor exhibits some unique

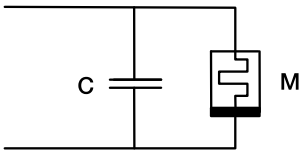

Fig. 4. Probes coupling to the plasma through a memristor with a parasitic capacitive element in parallel.

properties which enables memristive devices to be distinguished from non-memristive devices. The first indication of memristor-like behavior can be seen in the shape of the V–I characteristics where a memristor exhibits the unique property called "pinched hysteresis loop." This characteristic property is referred to as the fingerprint of a memristor [23]. When applying a voltage source $v(t) = A\sin(\omega t)$ we will see a V–I Lissajous curve, with two distinct values of the current, except from when it crosses. An ideal memristor is also expected to pass through the origin $I = 0, v = 0$ with a single value. However, a memristor can have a significant offset of the pinch point due to parasitic elements [24]. Another fingerprint of the memristor is the decrease of the hysteresis loop area [25] as the frequency increases, which tends toward a single-valued curve for $\lim f \to \infty$. Memristors are furthermore divided into two branches depending on whether the loop of I–V characteristics cross the in the origin and it will be referred to as a transversal memristor or if the slopes are touching and it will be referred to as a tangential memristor [25].

In the perspective of the memristor, the illustration of the probe coupling to the plasma, shown in Fig. 3, can be replaced equivalent circuit where the resistance is replaced by a memristor with a capacitive element in parallel, as shown in Fig. 4.

V. Numerical Setup

To examine the non-linear properties of the probe, a numerical study using Particle in Cell (PIC) model was accomplished. We used the PTetra model that was modified to support a time-varying bias. The PTetra model uses an unstructured grid and follows a standard PIC scheme, [26], [27]. The geometry and mesh were generated using the open-source meshing tool Gmesh [28]. Particles are initiated with Boltzmann distributed velocity given by, respectively, the ion- and electron temperature. The particles move in the defined volume by integrating the Lorentz force implemented as leap frog scheme giving a second-order accuracy. The model supports static magnetic fields. However, in this study, an external magnetic field is not considered.

The simulated probe is a sphere with a radius of 2 cm inside the computational volume limited by an outer sphere with a radius of 40 cm. The mesh was generated with an outer mesh resolution set to 4 mm and an inner resolution set to 2 mm. Fig. 5 shows the simulation setup. The probe bias was a sine wave with an amplitude of $+/-5$ V with the following frequencies: 5, 10, 20, 40, 80, 160, 320, and 640 kHz. The plasma temperature was in the range 0.2–1 eV in a quasi-neutral plasma with a density from 3.5×10^{11} to 28×10^{11} m^{-3}. The ions were all taken to be H^+ except for the simulations where heavier ions from 2 to 7 u were compared. To reduce noise and simulation time, a larger probe radius than normal was used. The size of the probe does not fulfill the requirements of the OML theory for spherical probes where $R \ll \lambda_D$, and we can expect a probe current between the current of a spherical probe and for a planar probe with the area of the sphere. Plasma parameters and parameters used in the simulations are listed in Table I.

TABLE I
Simulation and Central Parameters, Calculated for the Reference Case With a Frequency of 40 kHz

Parameter		Value
Electron density	n_e	7.0×10^{11} m^{-3}
Ion density	n_i	7.0×10^{11} m^{-3}
Electron temperature	T_e	0.2 eV - 2320 K
Ion temperature	T_i	0.2 eV - 2320 K
Electron Plasma period	$2\pi\omega_{pe}^{-1}$	0.13 µs
Ion Plasma period	$2\pi\omega_{pe}^{-1}$	5.68 µs
Debye length	λ_D	3.97 mm
Sheath formation time	τ_{sheath}	6 µs
Sheath capacitance	C_{sheath}	13.4 pF

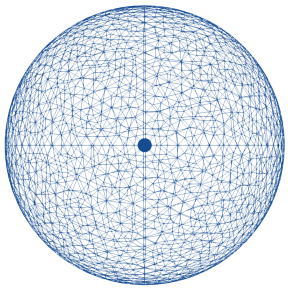

Fig. 5. Simulated probe is a sphere with a radius of 2.0 cm within the computational volume given by a spherical boundary with a radius of 40.0 cm. The mesh was generated using Gmesh with an outer mesh resolution set to 4.0 mm and an inner resolution set to 0.002 mm.

VI. Numerical Results

An initial study of a constant probe bias was performed to determine the sheath resistance without any capacitive effects. The probe was biased at 5 V and the simulation time was 20 μs. The data was filtered by a second-order Butterworth low-pass filter. At simulation start, the applied bias acts like a step-function, and the system needs time to stabilize. In Fig. 6 we can see that after about 1 μs, the current reaches a peak caused by the electrons in the immediate vicinity of the probe being attracted to the probe by the strong electric field. A steady-state condition is reached after about 10 μs and the average current over the last ion period is 492.6 μA.

In Fig. 7 we see the raw data compared to the filtered data for the 40 kHz simulation. The raw data is noisy and needs to be filtered. Any kind of filters applied will change the V–I characteristics either by introducing a phase delay, changing the hysteresis area, and/or moving the pinched point. Normally, an exponential averaging filter has been used to filter the PIC data. However, data in this model was filtered with a low-pass filter since this filter best preserved the shape of the signal in the V–I characteristics. The effect of the filter is a very small phase shift of the signal which also moves the pinched point of the hysteresis loop away from the origin of coordinates. The filter is constructed to filter the noise based on the time-step used in the PIC model and has a cutoff well

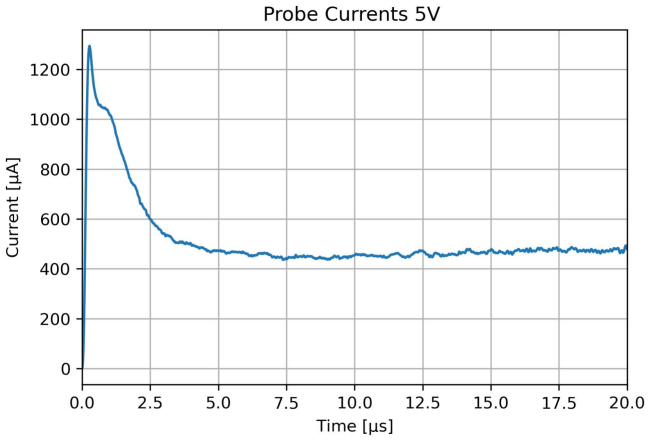

Fig. 6. Current to the probe as a function of time. The probe was biased fixed at 5 V and the simulation was run for 20 μs. Steady state is reached after about 10 μs.

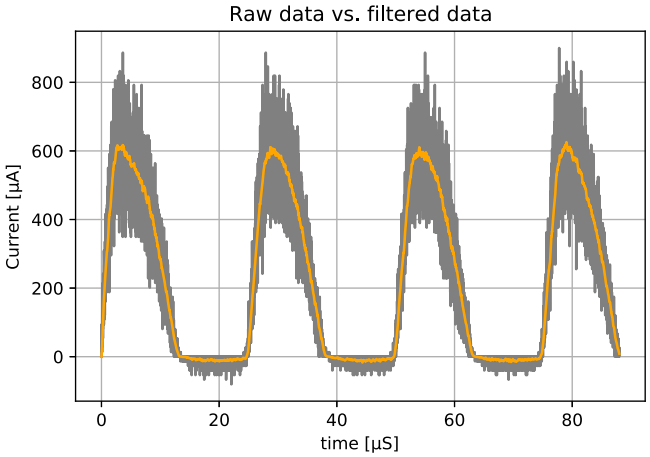

Fig. 7. Signal was filtered with a low-pass filter to reduce the noise.

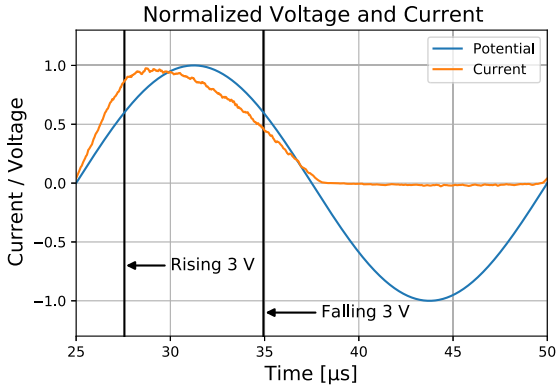

Fig. 8. Normalized amplitude of current and voltage for an applied 40 kHz sinusoidal probe bias. The ion current is small compared to the much larger electron current and there is the phase delay between the applied bias and the current. The current at rising probe bias is higher than at falling voltage.

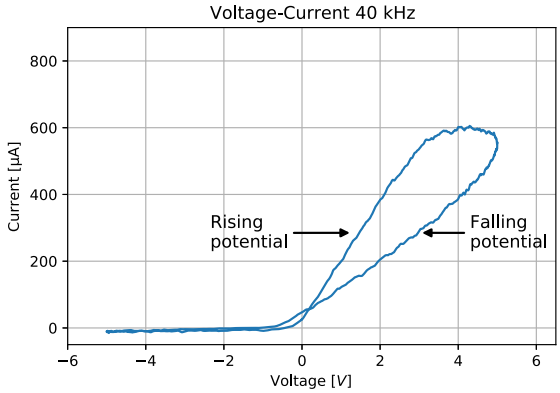

Fig. 9. V–I plot for 40 kHz. The upper line, with the highest current, is for the rising voltage, while the underneath line, with lower current, is for the falling voltage.

above the highest frequency used for the bias. The phase shift will be different for each frequency and is very small, within 1° or 2°. We simulated at least four periods for all frequencies, and we took the average over the last three periods after the cycle had stabilized.

A. Frequency Response

In our study, we have run simulations for sweeping signals from 5 up to 640 kHz. The V–I characteristics for the reference case at 40 kHz, with parameters given in Table I, is presented in Fig. 9. For the lowest frequencies considered in this study (5 and 10 kHz), the shape V–I characteristics is shown in Fig. 10. It is similar to the shape of the illustrated V–I characteristics in Fig. 1. We see a hysteresis in the electron saturation region with a higher current for the rising voltage than for the falling voltage. For the 5 kHz signal seen in Fig. 10, there are oscillations in the order of the ion period. As the frequency increases, the hysteresis in the electron saturation increases, and from 20 kHz we can see how the hysteresis also develops in the electron retardation region and stretches into the ion saturation. The formation time of the sheath, that acts like a resistance for the electrons, is according to (7), about 6 μs. Obviously the effect will also be present at shorter time intervals. For the case at 40 kHz, seen in Fig. 10, the probe is operated in the electron saturation region for about one quarter of the sweeping period, which corresponds to 6.25 μs, and from Fig. 8 we can see that the current is higher for the rising voltage than for the falling voltage. In Fig. 12 the simulated current is also compared to the theoretical capacitive current of the probe given by (12) and the theoretical capacitive current plus the steady-state current. We can see that the increase in current follows the tendency of the capacitive current, but is somewhat higher. This is as expected since the capacitive current should increase as frequency increases, and at the same time the resistive sheath has less time to establish, giving a smaller resistance and more electrons will be attracted toward the probe. However, the capacitive current is small for 40 kHz, so the difference in current for rising and falling bias should mainly be attributed to the sheath formation. This is further supported by the electron and ion density distributions in the vicinity of the probe as seen in Figs. 13 and 14, where we see a snapshot of the ion and the electron densities for the same rising and falling 3 V as marked in Fig. 8. We can see a higher density of the ions close to the probe for rising voltage than for falling voltage which illustrates that the ions need time to move out of the sheath region. Within the sheath, we also observe a

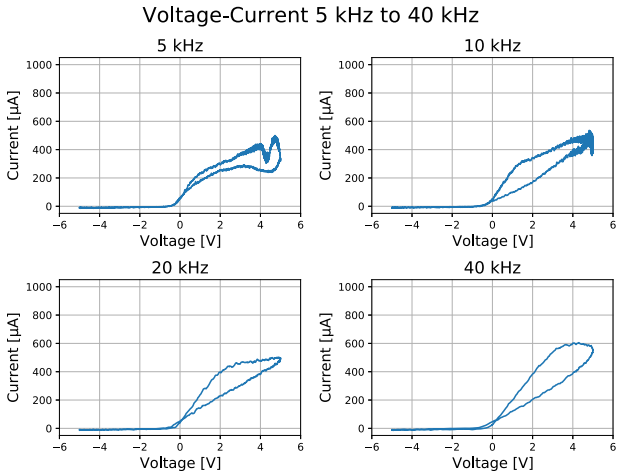

Fig. 10. V–I plot for frequencies from 5 to 40 kHz.

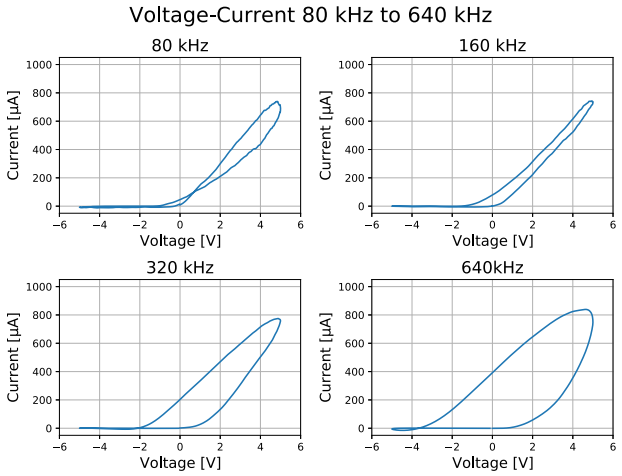

Fig. 11. V–I plot for frequencies from 80 to 640 kHz.

slightly lower density of electrons very close to the probe for falling than for rising bias. In total, the sheath has a higher density of electrons compared to the density of the ions that will slow down the electrons and reduce the current.

From Fig. 11, we see that the pinched curve vanishes in the electron saturation region as the frequency increases. The capacitive effect becomes more and more dominating and the current increases as demonstrated in Figs. 11 and 12.

B. Comparing Temperatures and Density

Since the current caused by the capacitive effect is dominated by the electrons, and since the sheath effects in the electron saturation region are dominated by the ions, it is reasonable to also examine the variation of the electron and ion temperatures separately. In Figs. 15 and 16 we compared the V–I characteristics for different electron and ion temperatures ranging from 0.2 to 1 eV. In Fig. 15 we see that the probe current is reduced when the electron temperature increases, in accordance with the current given by the OML theory in (3). While the thermal current increases by a factor of $\sqrt{T_e}$, the total current will decrease by a factor of $1/T_e$ when $1 \ll eV/kT$. This is an assumption for a steady-state condition when the capacitive effect will be absent. On the other hand,

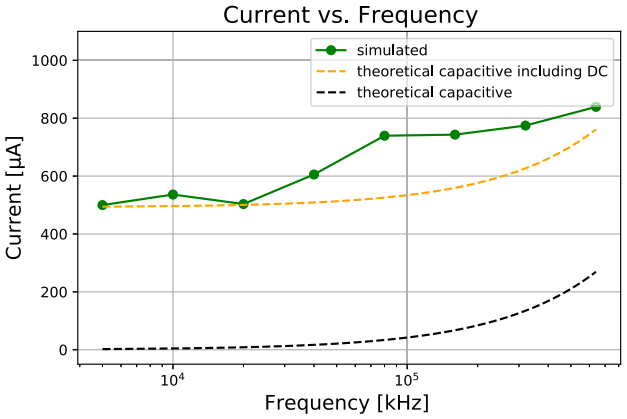

Fig. 12. Comparison of the simulated current to the theoretical capacitive current of the probe and to the theoretical capacitive current plus the simulated steady state current.

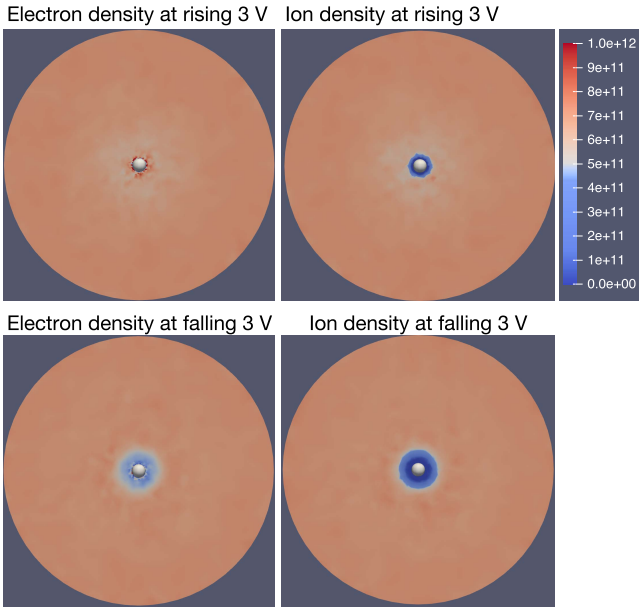

Fig. 13. Electron and ion densities at rising 3 V (top panels) and falling 3 V (bottom panels) bias voltage at 40 kHz. We can see that the ion density close to the probe is higher at rising bias than falling. The ions are pushed away and the sheath is formed. The positive potential in the sheath acts like a resistance and will slow down the electrons and reduce the current.

when we consider the current caused by the capacitive effect it will also be related to the temperature as seen in (13), and we see that current caused by the capacitive effects should also be reduced as the electron current is increased. However, as seen in Fig. 12 the capacitive current is small, about 17 μA for 40 kHz, and the current is less affected by the variation of the electron temperature than by the variation of the ion temperature.

From (7) it follows that the sheath formation time is reduced when the ion velocity is increased, which means that the sheath uses less time to build up and it will limit the current for higher temperatures. We also observe that when the temperature increases, the hysteresis area is shrinking and we are moving toward a linear curve. If we only increase the temperature of the electrons to 1.0 eV and keep the ions at 0.2 eV, there is a reduction of the current in accordance with (3) and (13), see Fig. 15. If the ion temperature is increased to 1.0 eV

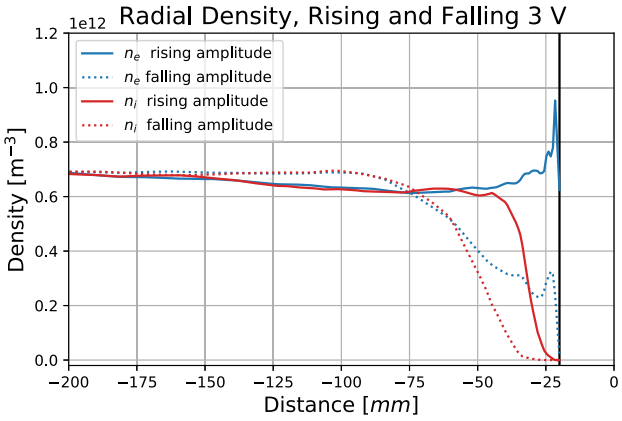

Fig. 14. Zoomed in radial electron and ion densities at rising 3 V and falling 3 V bias voltage at 40 kHz. The density is averaged over x-, y-, and z-direction. We can see how the ions have moved out of the sheath and electrons in the vicinity of the probe has been collected. The higher number of electrons are equaling out the potential from the applied probe bias.

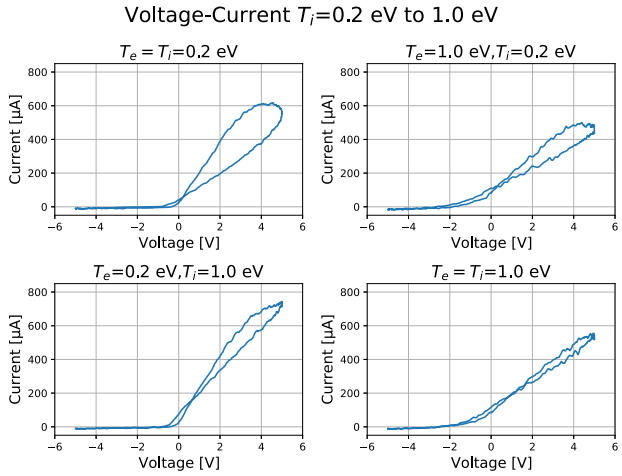

Fig. 15. V–I characteristics for different ion and electron temperatures ranging from 0.2 to 1 eV at 40 kHz.

and the electron temperature is at 0.2 eV, which is a situation that would be unlikely to occur in a real space environment, we see that the current increases. This is a bit unexpected since according to (7) the ions use less time to establish the sheath due to their higher mobility and we would expect that the sheath was established faster and the current should be reduced. However, since in this case $T_i > T_e$, the equations for the current to the probe would need to be revised.

As for the temperature, both the sheath capacitance and the steady-state current are related to the plasma density. According to the OML theory the thermal velocity is directly proportional to the density given in (4), and we can see this tendency in Figs. 17 and 18. In contrast to the electron temperature, the capacitive current will be proportional to the electron density given by (14) and the current will increase with density. However, as far as we know, this contribution is relatively small at 40 kHz.

C. Comparing Ion Masses

Simulations of ion masses from 1 to 7 u were performed. Ion masses heavier than 7 u resulted in instabilities and

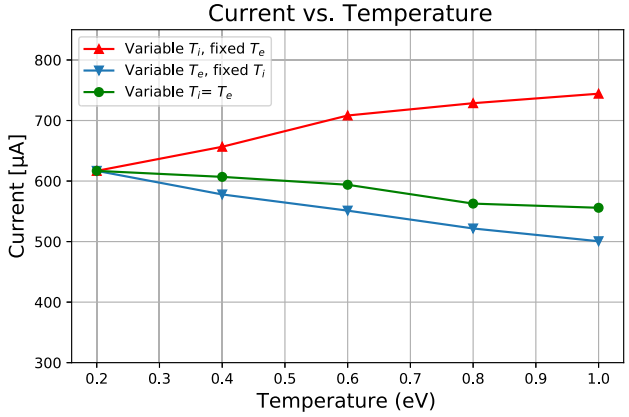

Fig. 16. Probe currents for different ion and electron temperatures. The red curve shows simulated currents for the ion temperatures from 0.2 to 1 eV while the electron temperature is fixed at 0.2 eV. The blue curve shows simulated currents for electron temperatures from 0.2 to 1 eV while the ion temperature is fixed at 0.2 eV. The green curve shows simulated currents for equal electron and ion temperatures ($T_e = T_i$) from 0.2 to 1 eV.

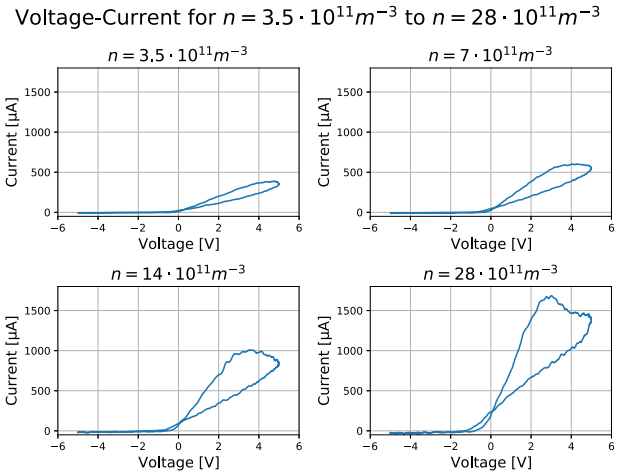

Fig. 17. V–I characteristics for densities from 3.5 10^{11} to 28 10^{11} m^{-3} at 40 kHz.

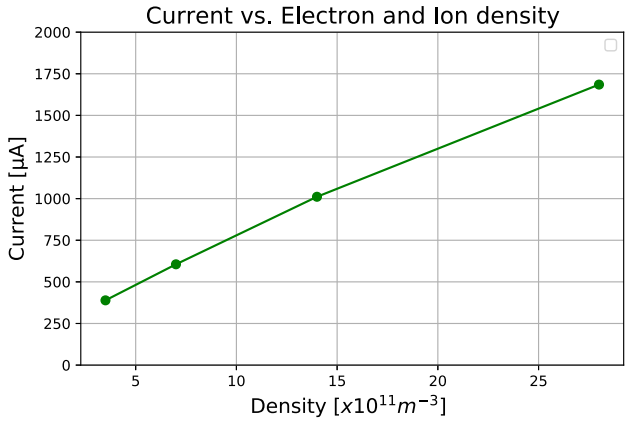

Fig. 18. Maximum probe currents for different densities ranging from 3.5 10^{11} to 28 10^{11} m^{-3}.

oscillations in the order of the ion plasma period and are not included. The sheath formation time given in (7) depends on the thermal velocity given in (8), which again depends on the ion temperature and the ion mass. In contrast to the

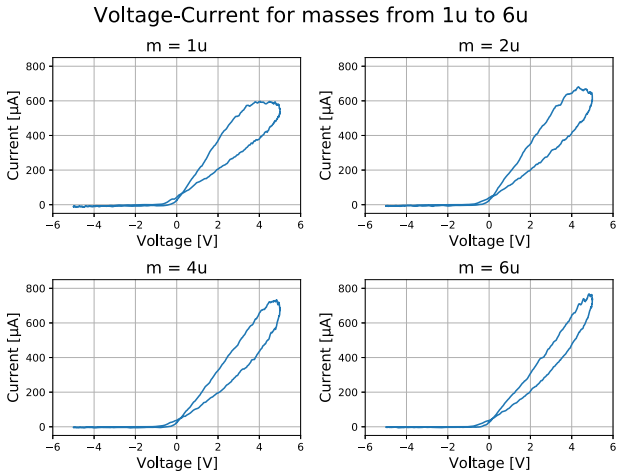

Fig. 19. V–I characteristics for ion masses of 1, 2, 4, and 6 u at 40 kHz. As the ion mass increases, the collected current increases and the hysteresis shrinks.

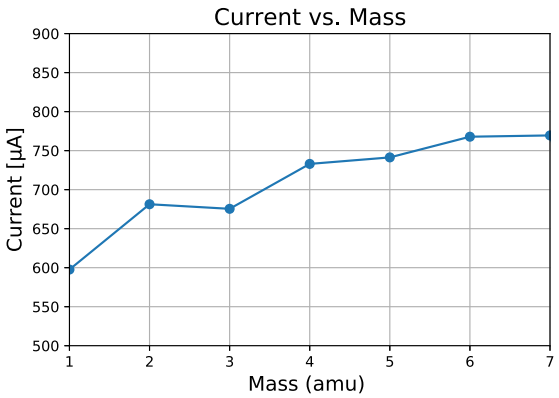

Fig. 20. Maximum probe currents as function of mass from 1 to 7 u. The current increases as the ion mass increases due to the longer formation time of the sheath and consequently less resistance.

change caused by varied temperatures, a higher ion mass will reduce the thermal speed, and the sheath formation time will increase as the ions use longer time to move out of the sheath region. Consequently, the resistance for the electrons will decrease, resulting in a higher current for heavier species as seen in Fig. 20. Since we know that the capacitive current mainly is associated with the electrons and it will remain unchanged here, the increase in the current for higher ion masses illustrates well how the sheath, and subsequently the resistance, needs time to build up. This is further supported by the reduction in hysteresis seen in Fig. 19 where the difference between rising and falling voltage is reduced.

VII. Discussion and Conclusion

Simulations carried out in this work disclose non-linear effects of a swept Langmuir probe with a pinched hysteresis loop and a double valued V–I characteristics. The hysteresis loop is an effect of sheaths that needs to form, as the ions needs time to move out of the sheath region. The hysteresis area will therefore depend on the frequency and shrink as the frequency is increased. As expected, we can see that the sheath formation time is dominated by the ions and the mobility of the ions related to the temperature and mass of the ions.

In the perspective of a memristor, this pinched hysteresis loop, with a double valued V–I characteristics, is the first fingerprint of a memristor exposed to a sinusoidal signal and as the V–I loop crosses it can furthermore be identified as a transversal memristor. Another fingerprint of the memristor is the decrease of the hysteresis loop area as the frequency increases, which tends toward a single-valued function. If we compare the results from 40, 80 and 160 kHz in Figs. 10 and 11 we see how the lobe area decreases and the pinched curve in the electron saturation region straightens out. We also see that sheath capacitance dominates as the frequency increases, and from 160 kHz the pinched curve vanishes, and we are left with the capacitive effect. In the context of a memristive circuit, the sheath capacitance can be introduced as a parasitic element parallel to the memristor as shown in Fig. 1. An effect of a parasitic element is that voltage and current cannot be equal to zero simultaneously [29] and as a result, the pinch point will not pass through the origin. It is also worth noticing that resistance in parallel or in series with the memristor is not discussed since the equivalent circuit itself will be a memristor [23].

The hysteresis measured in the V–I characteristics has commonly been contributed to surface contamination of the probe [11], [12]. In this study, we see that the hysteresis also can be attributed to the sheath and sheath formation time, determined by the mobility of the ions.

It is shown that a Langmuir probe immersed in plasma holds several non-linear properties that can be identified with a memristor. Non-linear effects for the swept Langmuir probes are a novel field and should be studied more systematically including experiments performed in a physical laboratory. A better understanding of the sheath formation process would particularly be very useful. However, the observed hysteresis and memristive properties illustrate the potential of swept Langmuir probe methods to disclose more of the plasma properties. A further study of these properties could possibly be used to introduce new measurement methods for characterization of plasma.

Acknowledgment

The simulations have been run at the Abel Cluster and the Sigma2 Cluster, owned by the University of Oslo, Oslo, Norway, and Uninett/Sigma2, Trondheim, Norway. The authors would like to thank Richard Marchand for making the PTetra model available.

References

[1] K. S. Jacobsen, A. Pedersen, J. I. Moen, and T. A. Bekkeng, "A new Langmuir probe concept for rapid sampling of space plasma electron density," *Meas. Sci. Technol.*, vol. 21, no. 8, Aug. 2010, Art. no. 085902. [Online]. Available: http://stacks.iop.org/0957-0233/21/i=8/a=085902

[2] E. Spencer and S. Patra, "Ionosphere plasma electron parameters from radio frequency sweeping impedance probe measurements," *Radio Sci.*, vol. 50, no. 9, pp. 853–865, 2015.

[3] A. Barjatya and C. M. Swenson, "Observations of triboelectric charging effects on Langmuir-type probes in dusty plasma," *J. Geophys. Res.*, vol. 111, no. A10, 2006, Art. no. A10302.

[4] P. Muralikrishna, L. P. Vieira, and M. A. Abdu, "Spectral features of E- and F-region plasma irregularities as observed by rocket-borne electron density probes from Brazil," *Revista Brasileira de Geofísica*, vol. 25, no. 2, pp. 115–128, 2007.

[5] B. M. Oliver, R. M. Clements, and P. R. Smy, "Experimental investigation of the low-frequency capacitive response of a plasma sheath," *J. Appl. Phys.*, vol. 44, no. 10, pp. 4511–4517, Oct. 1973.

[6] K. G. Balmain, "The impedance of a short dipole antenna in a magnetoplasma," *IEEE Trans. Antennas Propag.*, vol. AP-12, no. 5, pp. 605–617, Sep. 1964.

[7] K. Balmain, "Dipole admittance for magnetoplasma diagnostics," *IEEE Trans. Antennas Propag.*, vol. AP-17, no. 3, pp. 389–392, May 1969.

[8] H. Hoang *et al.*, "A study of data analysis techniques for the multi-needle Langmuir probe," *Meas. Sci. Technol.*, vol. 29, no. 6, Art. no. 065906, May 2018, doi: 10.1088%2F1361-6501%2Faab948.

[9] K. M. Kjølerbakken, W. J. Miloch, and K. Røed, "The influence of probe spacing and probe bias in a double Langmuir probe setup," *AIP Adv.*, vol. 11, no. 8, p. 085007–9, 2021.

[10] L. H. Brace, *Langmuir Probe Measurements in the Ionosphere*. Washington, DC, USA, 1998, pp. 23–35.

[11] K.-I. Oyama, *An Introduction to Space Instrumentation*. Shintoshin, Saitama: TERRAPUB, Nov. 2013, ch. Langmuir Probe, pp. 63–75.

[12] W. E. Amatucci *et al.*, "Contamination-free sounding rocket Langmuir probe," *Rev. Sci. Instrum.*, vol. 72, no. 4, pp. 2052–2057, Apr. 2001.

[13] K.-I. Oyama, C. H. Lee, H. K. Fang, and C. Z. Cheng, "Means to remove electrode contamination effect of Langmuir probe measurement in space," *Rev. Sci. Instrum.*, vol. 83, no. 5, p. 055113, 2012.

[14] P. Špatenka and H. Suhr, "Langmuir probe measurements during plasma-activated chemical vapor deposition in the system argon/oxygen/Aluminum isopropoxide," *Plasma Chem. Plasma Process.*, vol. 13, no. 3, pp. 555–566, Sep. 1993, doi: 10.1007/BF01465882.

[15] F. Chen, *Introduction to Plasma Physics and Controlled Fusion*, 3rd ed. Cham: Springer, 2016.

[16] W. J. Miloch, N. Gulbrandsen, L. N. Mishra, and Å. Fredriksen, "Ion velocity distributions in the sheath and presheath of a biased object in plasma," *Phys. Plasmas*, vol. 18, no. 8, Aug. 2011, Art. no. 083502, doi: 10.1063/1.3614520.

[17] H. M. Mott-Smith and I. Langmuir, "The theory of collectors in gaseous discharges," *Phys. Rev.*, vol. 28, pp. 727–763, Oct. 1926, doi: 10.1103/PhysRev.28.727.

[18] L. S. Pilling and D. A. Carnegie, "Validating experimental and theoretical Langmuir probe analyses," *Plasma Sources Sci. Technol.*, vol. 16, no. 3, p. 570, 2007. [Online]. Available: http://stacks.iop.org/0963-0252/16/i=3/a=016

[19] R. B. Lobbia and A. D. Gallimore, "Temporal limits of a rapidly swept Langmuir probe," *Phys. Plasmas*, vol. 17, no. 7, Jul. 2010, Art. no. 073502.

[20] S. A. Nikiforov, G.-H. Kim, and G.-H. Rim, "Dynamics of high-voltage pulsed cylindrical sheath," *IEEE Trans. Plasma Sci.*, vol. 31, no. 1, pp. 94–103, Feb. 2003.

[21] F. W. Crawford and R. Grard, "Low-frequency impedance characteristics of a Langmuir probe in a plasma," *J. Appl. Phys.*, vol. 37, no. 1, pp. 180–183, Jan. 1966.

[22] L. O. Chua, *Introduction to Nonlinear Network Theory*. New York, NY, USA: McGraw-Hill, 1969.

[23] L. O. Chua, "Memristor—The missing circuit element," *IEEE Trans. Circuit Theory*, vol. CT-18, no. 5, pp. 507–519, Sep. 1971.

[24] M. P. Sah, C. Yang, H. Kim, B. Muthuswamy, J. Jevtic, and L. Chua, "A generic model of memristors with parasitic components," *IEEE Trans. Circuits Syst. I, Reg. Papers*, vol. 62, no. 3, pp. 891–898, Mar. 2015.

[25] S. P. Adhikari, M. P. Sah, H. Kim, and L. O. Chua, "Three fingerprints of memristor," *IEEE Trans. Circuits Syst. I, Reg. Papers*, vol. 60, no. 11, pp. 3008–3021, Nov. 2013.

[26] R. Marchand, "PTetra, a tool to simulate low orbit satellite–plasma interaction," *IEEE Trans. Plasma Sci.*, vol. 40, no. 2, pp. 217–229, Feb. 2012.

[27] R. Marchand and P. A. R. Lira, "Kinetic simulation of spacecraft–environment interaction," *IEEE Trans. Plasma Sci.*, vol. 45, no. 4, pp. 535–554, Apr. 2017.

[28] C. Geuzaine and J.-F. Remacle, "Gmsh: A 3-D finite element mesh generator with built-in pre- and post-processing facilities," *Int. J. Numer. Methods Eng.*, vol. 79, no. 11, pp. 1309–1331, Sep. 2009.

[29] B. Muthuswamy *et al.*, "Memristor modelling," in *Proc. IEEE Int. Symp. Circuits Syst. (ISCAS)*, Jun. 2014, pp. 490–493.

Kai Morgan Kjølerbakken (Member, IEEE) received the M.Sc. degree in physics and the Ph.D. degree from the University of Oslo (UIO), Oslo, Norway, in 2001 and 2022, respectively.

Since 2014, he has also been a Scientist with the Norwegian Institute for Air Research (NILU), Kjeller, Norway. His research interests include computational physics, non-linear systems, machine learning, and audio.

Wojciech J. Miloch (Member, IEEE) received the M.Sc. degree in space and plasma physics and the Ph.D. degree from the University of Oslo, Oslo, Norway, in 2006 and 2009, respectively.

He is currently a Professor and the Head of the 4DSpace Strategic Research Initiative, Department of Physics, University of Oslo. His current research interests include space and astrophysical plasmas, space weather, plasma interactions with finite-sized objects (such as spacecrafts, probes, or dust grains), complex plasmas, and numerical modeling.

Ørjan Grøttem Martinsen (Senior Member, IEEE) received the Ph.D. degree from the Department of Physics, University of Oslo, Oslo, Norway, in 1995.

He is currently a Professor of electronics with the Department of Physics, University of Oslo; and holds an adjunct position as a Senior Researcher at the Department of Clinical and Biomedical Engineering, Oslo University Hospital, Oslo. He is the coauthor of the textbook *Bioimpedance and Bioelectricity Basics*. His research is mainly focused on electrical properties of biomaterials.

Dr. Martinsen is the Editor-in-Chief of the *Journal of Electrical Bioimpedance*.

Oliver Pabst (Member, IEEE) received the Diploma degree in electrical engineering from the Dresden University of Technology, Dresden, Germany, in 2013, and the Ph.D. degree in physics from the University of Oslo (UiO), Oslo, Norway, in 2018.

He is currently working as a Post-Doctoral Researcher with the Department of Physics, UiO. His research interests include memristors; linear and non-linear electrical measurements on human skin, cells, and other biological tissues; bioimpedance; bioelectricity; neuroscience; and proton conduction.

Ketil Røed (Member, IEEE) received the M.Sc. and Ph.D. degrees from the Department of Physics and Technology, University of Bergen, Bergen, Norway, in 2004 and 2009, respectively.

From 2009 to 2011, he was a fellow of the Radiation to Electronics (R2E) Project at CERN, Geneva, Switzerland, working on Monte Carlo modeling and monitoring of radiation environments. He is currently a Professor with the Department of Physics, University of Oslo, Oslo, Norway. His current research interests are sensors and instrumentation for high-energy physics and space applications, including radiation and space weather effects on electronics.